PHYSICAL REVIEW B VOLUME 44, NUMBER 13 1 OCTOBER 1991-I

Local structure of $BaBi_xPb_{1-x}O_3$ determined by x-ray-absorption spectroscopy

J. B. Boyce
Xerox Palo Alto Research Center, Palo Alto, California 94304

F. G. Bridges
Department of Physics, University of California, Santa Cruz, California 95064

T. Claeson
Physics Department, Chalmers University of Technology, S-412 96 Göteborg, Sweden

T. H. Geballe
Department of Applied Physics, Stanford University, Stanford, California 94305

G. G. Li
Department of Physics, University of California, Santa Cruz, California 95064

A. W. Sleight
Department of Chemistry, Oregon State University, Corvallis, Oregon 97331-4003
(Received 26 April 1991)

X-ray-absorption fine-structure (XAFS) spectroscopy was employed to study the near-neighbor environments of the Bi and Pb atoms in the perovskite-structured material $BaBi_xPb_{1-x}O_3$, for $x=1$, 0.75, 0.5, and 0.25. For the semiconducting end member, $BaBiO_3$, two Bi-O distances, separated by 0.18 Å, could be distinguished, consistent with diffraction results. After alloying with Pb, two Bi-O distances are still observed in the semiconducting alloys ($x=0.75$ and 0.50) as well as in the metallic and superconducting phase ($x=0.25$). In all the alloys, the two Bi-O distances and their separations decrease somewhat with increasing Pb concentration. The weighted average of the Bi-O and Pb-O distances is consistent with half the pseudocubic cell edge ($V^{1/3}$) determined from diffraction. The different Bi-O bond lengths are accompanied by charge-density fluctuations which may enhance local, breathing-type phonon modes and thereby increase the coupling between electron and phonon states. For the metallic and superconducting phase, these fluctuations are consistent with a local charge-density-wave picture and the presence of a pseudogap. These results may have implications for the superconductivity, with a relatively high T_c, in these oxides.

I. INTRODUCTION

Two different Bi sites and two distinctly different Bi-O distances have been found in $BaBiO_3$ by neutron diffraction.[1-4] This has led to a suggestion of valence disproportionation, $Ba_2(Bi^{3+}Bi^{5+})O_6$, giving the preferred valences of 3+ and 5+ for Bi instead of the mean value of 4+, which is unfavorable for Bi and not generally found in chemical compounds. However, x-ray photoemission spectroscopy[5,6] and photoemission[7,8] measurements of the electronic structure, as well as band-structure calculations,[9] do not give any appreciable amount of charge transfer. In a previous study,[10] we have shown that x-ray-absorption fine-structure (XAFS) measurements were able to separate two distinctly different Bi-O distances, but the near-edge structure gave no clear evidence for a mixture of 3+ and 5+ valences. Heald *et al.*[11] could find no evidence of any significant amount of disproportionation into two Bi valence states and concluded that the valence is 4+. Contrary to these conclusions, there is a claim[12] of two Bi valences based on broadened absorption spectra similar to those observed in the previous work mentioned above.[10,11] There are indications of charge-density ordering of holes on O sites instead of on Bi sites.[6,11] This is analogous to the importance of holes on the O for the high-T_c copper oxides. In $BaBiO_3$, the Bi-O bond is more covalent than ionic in character.[8] As a result, it should be emphasized that the fluctuating charge would be located somewhere between the Bi and O ions, with a possible preference towards the O site. Hence, 3+ and 5+ for Bi should be interpreted as formal charges, not absolute charges.

The question is what happens when Pb is alloyed into $BaBiO_3$. The perovskite-type lattice remains[13] for all Pb compositions in $BaBi_xPb_{1-x}O_3$. It has a monoclinic distortion for $x>0.9$, orthorhombic for $0.35<x<0.9$ and $x<0.1$, and tetragonal for $0.1<x<0.35$. The tetragonal phase corresponds to the superconducting phase, and those with $x>0.35$ are semiconducting. One might expect the end member compound $BaBiO_3$ to be a good metal with a half-filled conduction band. However, it is a

semiconductor. An accepted model is that frozen Bi-O stretching modes ("breathing" modes where the O environment as a whole moves in or out relative to the two inequivalent Bi sites) induce a distortion of the perovskite structure and give rise to a static charge-density wave (CDW). The transformation to a doubled unit cell, with an energy gap at the Fermi surface and a semiconducting state, is thought[9] to be of the Peierls type. Alloying with Pb should destroy the long-range order of the CDW and restore metallic conductivity. However, the semiconducting state remains until 65% of the Bi atoms have been replaced by Pb. Then the Pb wave-function overlap is large enough that the alloy becomes metallic and superconducting.[13] The nonmetallic state, at lower Pb concentrations, has been proposed to be due to a local CDW ordering.[14–17] The scattering due to alloying on the conducting (Bi,Pb)-O-(Bi,Pb) chains will also promote localization, so one may consider the bands to be a mixture of itinerant and localized electrons. The localization of electrons in Bi-O bonds will tend to make the Bi electron band narrow. With two different bonds (i.e., different bond lengths and charge distributions), the Bi-O electron band will split into two bands with a band gap. In the metallic state, the tendency for two different bands may result in a dip in the density of state in the center of the band.

Optical reflectivity measurements[18] give a maximum in the optical conductivity at 2 eV, for $0.8 < x < 1$, the semiconducting phase. This has been ascribed to a CDW gap which decreases as the Bi concentration is decreased below $x = 0.8$. The peak in the optical conductivity versus frequency, i.e., the optical energy gap, does not disappear at the semiconductor-to-metal transition at $x = 0.35$ and is observed down to $x = 0.2$. Hence, one claims that a pseudogap remains in the metallic state for $0.2 < x < 0.35$. It may be connected to a sharp dip in the density of states at the Fermi level, a remnant of the CDW gap observed for $x = 1$. Our previous experiments[10,19] gave support for two different Bi-O separations, not only in $BaBiO_3$, but also in superconducting $BaBi_{0.25}Pb_{0.75}O_3$.

The advent of superconductivity,[20] with T_c higher than 30 K in the potassium-doped $BaBiO_3$ ($Ba_{1-x}K_xBiO_3$ for $0.3 \leq x \leq 0.5$; with $x = 0.4$ having optimum $T_c \simeq 30$ K), aroused substantial interest in the doped bismuth oxides. T_c is of the same order as for Sr- and Ba-doped La_2CuO_4, a high-T_c cuprous oxide. There are many similarities between the cuprous and bismuth oxides, but also differences. As there is no consensus on the mechanism of superconductivity in the copper oxides, work on related systems that may elucidate the situation is of great importance. In contrast to the results for the $Ba(Bi,Pb)O_3$ system, XAFS (Refs. 11, 21, and 22) gives only one Bi-O separation in the metallic state of $(Ba,K)BiO_3$. The optical gap decreases with K concentration and goes to zero at the semiconductor-to-metal transition.[23] There is no pseudogap in the metallic state.

It is the purpose of this work to more fully study the near-neighbor environments of both the Bi and Pb atoms in $BaBi_xPb_{1-x}O_3$ as x is varied from 0.25 to 1 through the metal-semiconductor transition. We employ XAFS which is sensitive to the local structure, and use an extraction procedure to subtract the contribution of the strongly interfering Pb-edge XAFS from the Bi-edge XAFS.

The results may have implications on the understanding of high-temperature superconductivity in oxides. $BaBi_{0.25}Pb_{0.75}O_3$ is a superconductor with a transition temperature ($T_c \approx 13$ K) that is much higher than expected from its charge carrier density.[9,24] Although the superconductivity may still be explained within the context of an (possibly enhanced) electron-phonon coupling mechanism,[25–27] there have been several explanations with alternate mechanisms.[17,28–34] To a large extent, they are based on charge-density waves or fluctuations. Recent theoretical work[27] indicates that the electron-phonon mechanism may explain the $T_c = 30$ K of the $(Ba,K)BiO_3$ superconductor. Surprisingly enough, however, this theory gives too low a T_c for the $Ba(Bi,Pb)O_3$ system.

In Sec. II we describe the experimental details and present the data-reduction procedure in Sec. III. The general results are given in Sec. IV for both the Pb- and Bi-edge data. Section V describes the extraction of the Bi local environment and Sec. VI discusses these results. A summary is presented in Sec. VII.

II. EXPERIMENT

Samples of composition $x = 0.25$, 0.5, 0.75, and 1 were prepared[1] by heating appropriate mixtures of oxides, carbonates, and nitrates in air at 800–1000 °C. For the XAFS measurements, a crushed, fine power was brushed onto tape. The thickness was about 2 absorption lengths at the Bi L_{III} edge. The tape strips were mounted in He exchange gas in a nitrogen cryostat and measured at 80 K. Our previous study[10] on a different set of samples from another laboratory did not give any measurable difference between fine and coarse powder prepared a few days before or immediately before the measurements. So, substantial errors due to oxygen depletion can be ruled out. In this study, we used only fine powder.

The experiments were performed at the wiggler beamline IV-1 of the Stanford Synchrotron Radiation Laboratory. The Si(220) monochromator was detuned to $\frac{1}{2}$ maximum intensity in order to reduce harmonic reflections. The incident and transmitted intensities were recorded with nitrogen gas in the ionization counters. The monochromator energy was monitored for each scan using Pb foil or $BaBiO_3$ powder as a reference. The reference sample was placed between the transmitted-intensity counter and a third ionization chamber. Slits (0.7×5 mm) limited the incident photon beam. The energy resolution for our running conditions [0.7-mm slit, 13-keV energy, Si(220) monochromater, Stanford Synchrotron Radiation Laboratory (SSRL) beamline IV-1] was about 3 eV. Photographs were taken to insure that there were no pinholes in the samples.

Data were taken at the Pb L_{III} (13.035 keV) and Bi L_{III} (13.418 keV) edges. For the alloys, the analysis of the Bi

L_{III} data was complicated by the fact that the Pb and Bi L_{III} edges are close ($\Delta E = 383$ eV). The Pb XAFS oscillations extend above 13.418 keV ($k \simeq 10$ Å^{-1}) and must be subtracted before processing the Bi-edge data. A new procedure, described below, was used to successfully extract the Bi XAFS.

III. XAFS DATA REDUCTION

The data was reduced[35] in order to enable a quantitative comparison with standards to extract numbers for the near-neighbor distances, R_j, the Debye-Waller-type broadening of that distance, σ_j, and the number of neighbors, N_j, in shell j around the absorber. First, the slowly varying prethreshold background absorption was subtracted to yield the absorption due to the atom of interest. Next, the background above the edge was fit to a series of splines and the XAFS function, $\chi(E)$, was determined. $\chi(E)=[\mu(E)-\mu_0(E)]/\mu_0(E)$, where the absorption cross section $\mu(E)$ includes both the absorption edge and the XAFS oscillations and $\mu_0(E)$ is the free atomic absorptance. Finally, the data were transformed to k space ($\hbar^2k^2/2m_e = E - E_0$, where E_0 is the energy at one-half the absorption edge height). The resulting XAFS function

$$k\chi(k)=\sum_j \{N_jF_j(k)\sin[2kR_j+\phi_j(k)]\exp(-2k^2\sigma_j^2-2R_j/\lambda_j)\}/R_j^2$$

contains the desired structural parameters R_j, N_j, σ_j, as well as the XAFS response parameters, the phase shifts ϕ_j (depending on both the absorber and scatterer), scattering amplitudes F_j, and the electron mean free path λ_j.

Next, the XAFS in wave-vector (k) space is Fourier transformed to real (r) space, using as long a k interval as possible. A qualitative picture of the radial distribution of neighbors can then be perceived by inspecting these Fourier transforms of the XAFS oscillations. However, to obtain numerical values for R_j, N_j, and σ_j, we have performed least-squares fits to the real and imaginary parts of the Fourier transform of $k\chi(k)$. In these fits we have generally used experimentally determined standards. In this case, compounds with well-defined neighbor environments were measured at a low temperature. The contributions to a peak from further neighbors were subtracted to obtain a data file that corresponds to a peak for a single pair of atoms. For example, there is significant overlap in the XAFS of the Pb-O first neighbors and the Pb-Pb second neighbors for the Pb central atoms in β-PbO_2. The Pb-Pb peak must be subtracted to arrive at a Pb-O peak undistorted by contributions from the Pb second neighbors. In cases where structural standards were not readily available, data from a pair of atoms with atomic numbers near those for the atoms of interest were collected and modified using theoretical curved-wave calculations to represent the desired pair.

For Pb-O, we have used β-PbO_2 data taken at 4.2 K, and subtracted the contribution of the second-neighbor Pb-Pb peak. β-PbO_2 is tetragonal ($a = 4.961$ Å and $c = 3.385$ Å) and the Pb atoms have four O neighbors[36] at 2.140 Å and two at 2.176 Å (at room temperature). A single-distance Pb-O standard can be constructed from the XAFS of β-PbO_2 by removing the multipeak phase using this known structure, assuming comparable widths for the two components. This yields a Pb-O standard with six oxygen atoms at the average distance of 2.164 Å. The procedure is described in Ref. 37.

For Bi-O, we used the above Pb-O standard and modified it using the theoretical calculations[38] to account for the different central-atom phase shift from Pb ($Z = 82$) to Bi ($Z = 83$). This method is described in Ref. 39. We should note that Bi_2O_3 has a complicated crystal structure with several interfering Bi-O distances. Hence, we have not used it for XAFS evaluations but only for edge comparisons.

To determine a standard for the (Pb,Bi)-Ba second neighbors, we used Hg L_{III} data from HgTe. As described above, the central atom phase for Hg ($Z = 80$) was modified using spherical wave calculations[38] to yield those for Pb ($Z = 82$) and Bi ($Z = 83$) central atoms. Likewise, the backscattering phase and amplitude were modified from those of Te ($Z = 52$) to those for Ba ($Z = 56$). For the third neighbor, Pb-(Pb,Bi), a standard was extracted from Pb foil and also from Au foil using the spherical wave calculations to account for the small difference in Z. These two Pb-Pb standards agreed well except that the peak width from the Pb foil is considerably larger, as expected for this soft material. A Bi-Bi standard was generated from this Pb-Pb reference.

IV. GENERAL RESULTS

The main complication in this experiment is the closeness in energy of the Pb and Bi L_{III} edges. The short energy range between these edges limits the available k-space range for the Pb edge data to $k < 10$ Å^{-1}. The x-ray absorption as a function of energy is shown in Fig. 1 for the four compositions, and it is clear that the Pb XAFS is still strong at the Bi edge, particularly for the 25% Bi sample. For this superconducting alloy, the Pb content and absorption are three times larger than those for Bi, and the Pb background causes a substantial difficulty for the extraction of fine details from the Bi data. We first present the Pb edge data and its analysis before discussing the more detailed data reduction process for the Bi edge measurements.

A. Pb edge

In Fig. 2(a) we show $k\chi(k)$ for the Pb L_{III} edge of the 75% Pb sample. The sharp upturn of the k-space data near 10 Å^{-1} is the beginning of the Bi L_{III} edge, limiting

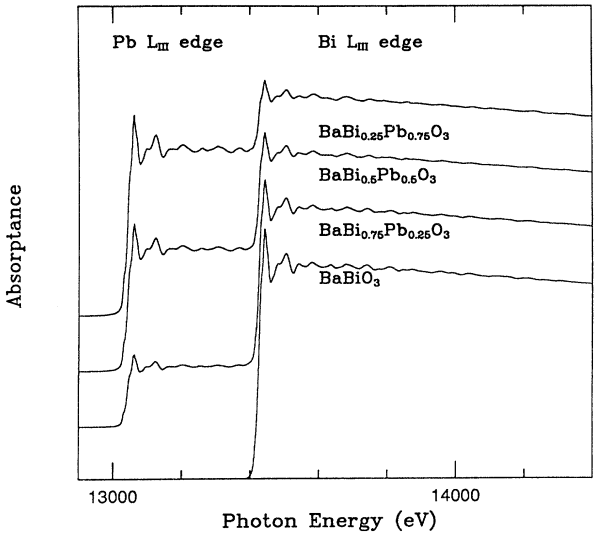

FIG. 1. The x-ray absorption of $BaBi_xPb_{1-x}O_3$, $x=0.25$, 0.5, 0.75, and 1, in the vicinity of the L_{III} edges of Pb (13.035 keV) and Bi (13.418 keV). The data were collected at 80 K. Note that the XAFS above the Pb edge is still strong at the Bi edge and will interfere with the XAFS of the latter.

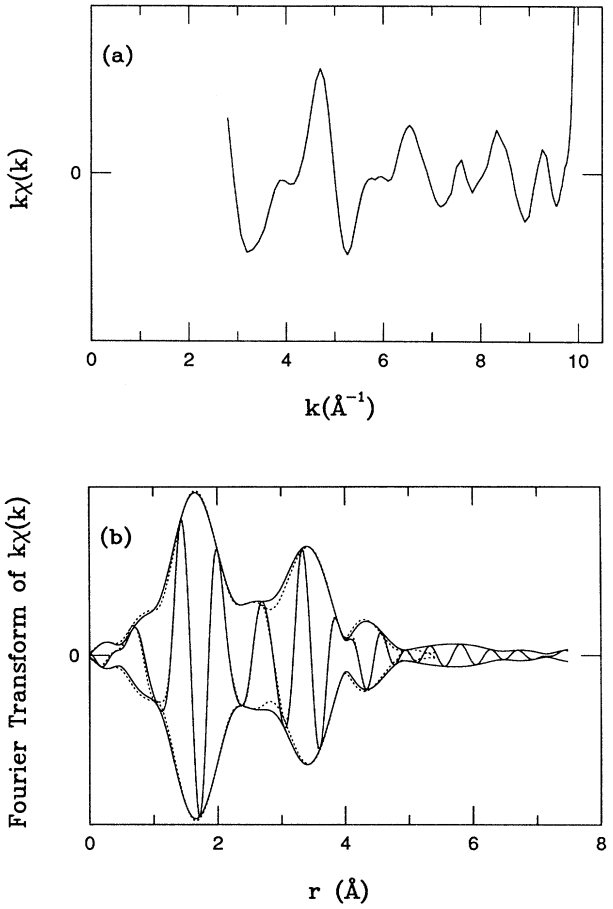

FIG. 2. XAFS at the Pb L_{III} edge for $BaBi_{0.25}Pb_{0.75}O_3$ in (a) k space and (b) real space. The r-space data have been transformed using a k-space window of 3.5–8.5 Å^{-1}, Gaussian broadened by 0.3 Å^{-1}. Both the real part and the absolute value (envelope curve) of the transform are shown. The dotted line in (b) is a fit to this data from 1.3 to 4.6 Å, including the Pb-O, Pb-Ba, Pb-(Bi,Pb) and long Pb-O peaks, as described in the text.

the range of the Pb-edge data. The data for the other compositions are very similar. In Fig. 2(b), we show the Fourier transform of this data using a window from 3.5 to 8.5 Å^{-1}, rounded by a Gaussian function with a half width of 0.3 Å^{-1}. In this plot we show the real part of the transform as well as the envelope function, i.e., the magnitude of the complex transform. This r-space data was fit to a sum of four standard peaks: Pb-O (nearest neighbor), Pb-Ba, Pb-(Bi,Pb), plus a further-neighbor Pb-O peak, over the range 1.3–4.6 Å in r space. We used a single peak for the third component since the sample contains 75% Pb and the Pb-Pb and Pb-Bi standards are quite similar. Likewise, we use a single broad Pb-O peak for the further O neighbors, although a range of distance is expected. In principle, further neighbors might also be fit, but the short k range available limits the number of parameters that can be extracted.

The resulting good fit to the r-space data is shown by the dotted line in Fig. 2(b), and the results for the near-neighbor distances are the following: $d_{\text{Pb-O}}=2.16$ Å, $d_{\text{Pb-Ba}}=3.70$ Å, $d_{\text{Pb-Pb}}=4.35$ Å, and $d_{\text{Pb-O}}=4.78$ Å, all in reasonably good agreement with the diffraction results of Ref. 3. The nearest-neighbor Pb-O and the Pb-Ba peaks fit very well; however, the fits for the Pb-(Bi,Pb) and the long Pb-O peaks are softer for two reasons. First, the Pb-(Bi,Pb) peak is really a sum of peaks, and, in addition, a multiscattering correction should be included for the intervening O atoms. Second, because the (broad) long Pb-O and Pb-(Bi,Pb) peaks overlap extensively, the parameters are coupled. Consequently, there is some uncertainty in their amplitudes and Debye-Waller factors.

For the oxygen shell about the Pb, we also compared fits using (i) one Pb-O peak and (ii) two Pb-O peaks, over the r-space range 1.3–2.0 Å. We find that using a sum of two standards does not significantly improve the goodness of fit, and conclude that the Pb-O peak is well described by a single broadened peak. We note, however, that a short k-space range plays an important role and limits the separation of peaks that can be resolved. To test how well two peaks can be resolved for various k-space ranges, we simulated a two peak Pb-O shell, using two standards separated by 0.18 Å, and then applied our nonlinear least-squares-fitting routine. When the upper end of the k-space range is greater than approximately 11 Å^{-1}, the two peaks are easily resolved; however, when the range is decreased to 9 Å^{-1}, a single peak fits as well as two peaks. The broadened Pb-O peak obtained in our fits indicates that some disorder is present in this bond length. This disorder may be the result of disorder on the Bi sites.

B. Bi edge

For the Bi-edge results, a correction must be made for the remaining Pb-edge oscillations to enable a quantitative analysis of the Bi near-neighbor environment. This correction is very small for the 75% Bi sample but relatively large for the 25% Bi alloy. As an example, we show in Fig. 3 the steps for removing the Pb-edge oscillations from the Bi-edge data for the $x=0.25$ sample.

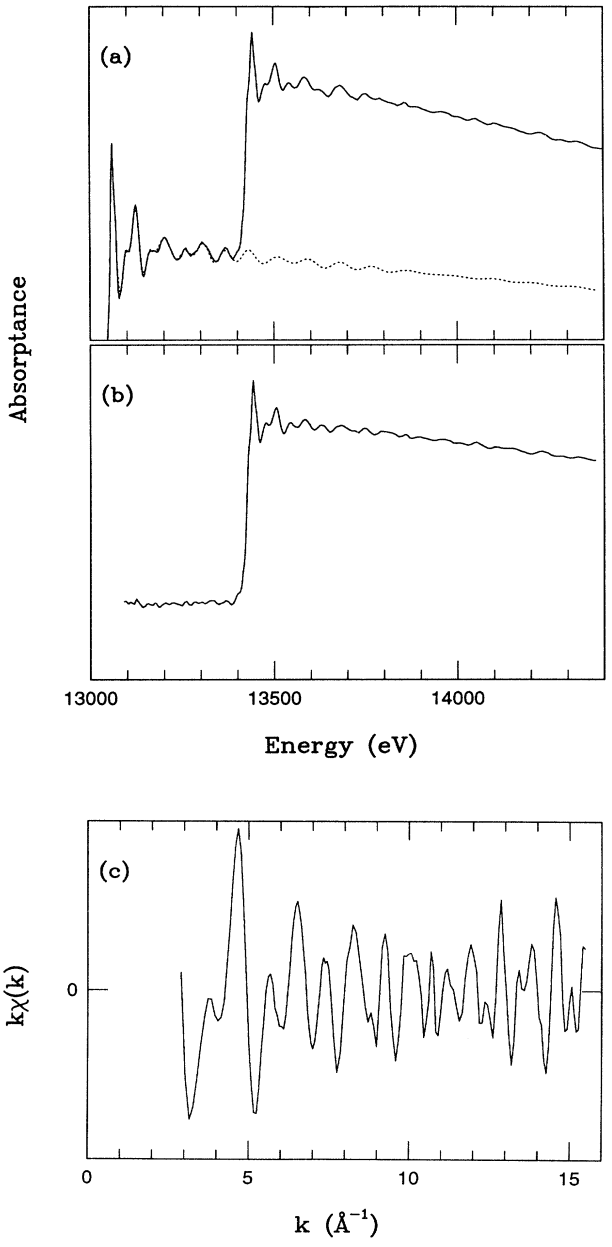

FIG. 3. (a) The x-ray absorption of $BaBi_{0.25}Pb_{0.75}O_3$ in the vicinity of the L_{III} edge of Bi showing the fit and extrapolation of the Pb-edge XAFS (dotted curve), determined as discussed in the text. (b) The Bi-L_{III} edge data after the subtraction of the Pb-edge contribution. (c) The resulting k-space data for the Bi edge extracted from the energy-space data shown in (b).

First, the data is processed to remove the background below the Bi-edge step; the Bi preedge region clearly shows Pb-edge oscillations [Fig. 3(a)]. Next, the results from the Pb-edge analysis above (the amplitude, position, and width of each of the peaks) are used to generate a long Pb-edge k-space ($k=19$ Å^{-1}) file as a sum of standard fields. This file is then converted back to energy space using the usual relationship between E and k, plus the Pb-edge energy, $E_0=13.035$ keV. Since the Pb data are normalized to the Pb-edge step height, the amplitude of this generated file must be adjusted before subtracting it from the Bi-edge data. This is achieved by determining the overall amplitude in a fit of the generated file to the Bi-preedge data. This eliminates estimating the amplitude factor from the ratio of the step heights or leaving it as a free parameter in the later fits of the Bi data. The resulting file to be subtracted from the Bi-edge data is shown as the dotted line in Fig. 3(a). The results of this subtraction are shown in Fig. 3(b). Note that the resulting Bi-preedge region is quite flat with some high-frequency noise, indicating that most of the low-frequency Pb oscillations have been removed. This corrected data is then processed in the usual way to obtain the Bi-edge k-space data presented in Fig. 3(c).

To gain some insight as to the effects of the background Pb oscillations, it is useful to consider the results in r space. First, we show in Fig. 4(a) the Fourier transform of the uncorrected data for the 25% Bi sample where the background problem is largest; again, we have plotted the real part of the transform as well as the envelope function. The overall amplitude is considerably larger than expected for this material and a large extra peak appears at 2.5 Å as a result of the background Pb-edge oscillations. The contributions from the Pb edge to the raw Bi data in Fig. 4(a) are illustrated in Fig. 4(b) for the first three Pb neighbors: Pb-O (solid curve), Pb-Ba (dotted curve), and Pb-Bi (long-dashed curve). The contribution from the long Pb-O bond is negligible at the Bi edge and has been omitted. Note that the Pb background is nearly 30% of the Bi-O peak amplitude. To generate these curves in Fig. 4(b), the long k-space file for each nearest-neighbor shell standard for the Pb is Fourier transformed, with a shift in E_0 to correspond to the Bi L_{III} edge. This effectively shifts all the Pb peaks to a lower value of r, and broadens them as a result of the square-root dependence of k on $(E-E_0)$. Most importantly, the phase of the real (and also the imaginary) part of the Fourier transform oscillates very rapidly with r, much faster than is usual in XAFS data. As a result, there is strong constructive and destructive interference between the Pb-Ba and the Pb-Bi components which result in a peak in the uncorrected data [Fig. 4(a)] at 2.5 Å and rapid oscillation of the real part of the transform in the range 2–3 Å. We can, therefore, add an additional constraint in the fitting of the Pb-edge data: the interference peak in the Bi data at 2.5 Å and the fast oscillations of the real part of the Fourier transform should be minimized. We find that these two features are quite sensitive to the widths and the positions of the Pb-Ba and Pb-Bi peaks. We stepped the Pb-edge fit parameters over a small range and each time recalculated the Bi-edge re-

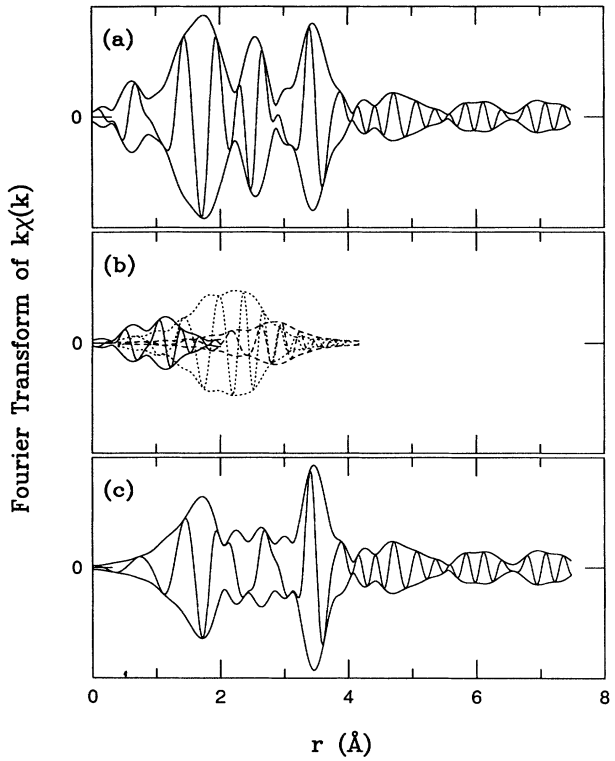

FIG. 4. (a) The real-space XAFS of $BaBi_{0.25}Pb_{0.75}O_3$ on the L_{III} edge of Bi, including the interfering contribution from the Pb L_{III} edge. (b) The Pb-edge contribution, determined as described in the text. Three contributions are shown: Pb-O, solid curve; Pb-Ba, dotted curve; Pb-(Bi,Pb), long-dashed curve. (c) The resulting r-space data on the Bi edge after the subtraction of the Pb contribution.

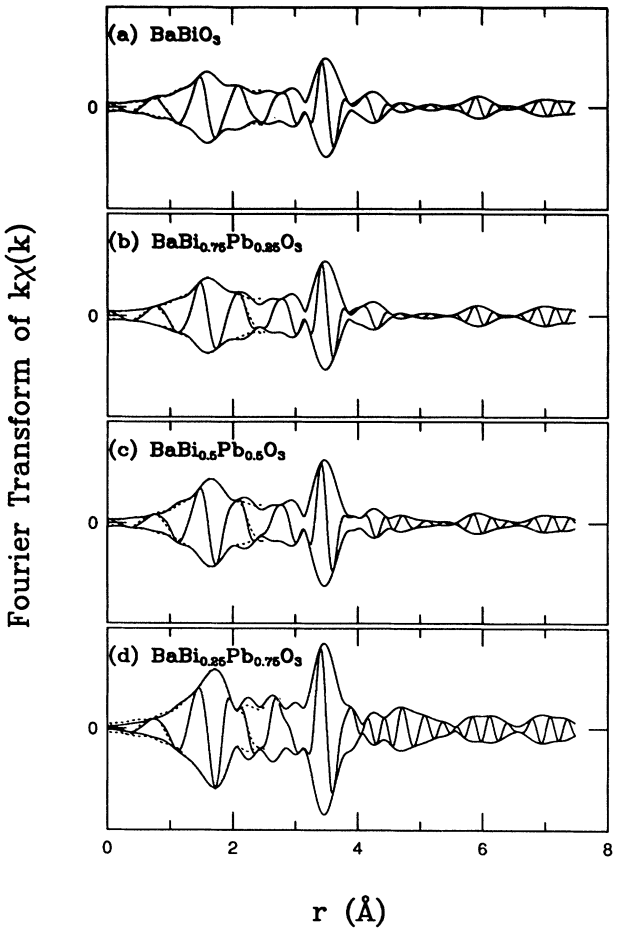

FIG. 5. XAFS in r space on the Bi L_{III} edge after the contribution from the Pb L_{III} edge has been removed for (a) $BaBiO_3$, (b) $BaBi_{0.75}Pb_{0.25}O_3$, (c) $BaBi_{0.5}Pb_{0.5}O_3$, and (d) $BaBi_{0.25}Pb_{0.75}O_3$. Both the real part and the magnitude (envelope curve) of the transform are shown. The transform range was 3.6–13.0 $Å^{-1}$, Gaussian broadened by 0.3 $Å^{-1}$. The fits in the range 1.3–2.2 Å, discussed in the text, are shown as dotted curves.

sults. This procedure minimizes the interference peak, yielding the results shown in Fig. 4(c). We note that this fine tuning of the fit has only a very small change in the corrected data below 2.0 Å, the Bi-O peak.

In this correction process, only the first three major peaks of the Pb data are included. Further Pb neighbor peaks, corresponding to more distant Ba and (Pb,Bi) neighbors, would result in additional peaks in Fig. 4(b) above $r = 3$ Å. For this sample, with three times more Pb than Bi, the correction that is made is relatively large. The correction for the 50% sample (equal amounts of Bi and Pb) is three times smaller and for the 25% Pb sample (Pb concentration $\frac{1}{3}$ that of Bi) it is nine times smaller. Good fits are not achieved in subsequent fits (see Sec. V) without this correction for the 50 and 75 % Pb samples.

In Fig. 5, we show the r-space results for all the alloys, with the above corrections applied, along with the data on the pure material, $BaBiO_3$. Three points to note are the following.

(1) The first peak near 1.8 Å in Fig. 5 corresponds to the O neighbors, and it clearly increases in amplitude as the concentration of Pb increases. We consider this peak in more detail below.

(2) The rest of the data out to 7 Å are very similar for the first three traces, although there are differences in the 50% sample, particularly above 4.5 Å.

(3) In the 75% Pb sample, the lack of a correction for the further Pb neighbors changes the resulting Bi-edge data significantly above 3 Å. Our simulations of the data for this case, our fits to the Pb edge, and the results of the subtraction shown in Fig. 4(c) indicate that 90–95 % of the Pb-edge background is removed in the region of the O peak 1–2 Å.

V. EXTRACTION OF THE PARAMETERS FOR THE Bi EDGE

The r-space data shown in Fig. 5 has several peaks corresponding to the different shells of Bi neighbors. These data are the Fourier transform of the k-space data, with a

Fourier transform range of 3.6–13.0 $Å^{-1}$, and have not been corrected for phase shifts which typically move the XAFS r-space peak position down by 0.3 to 0.5 Å. For the pure material, $BaBiO_3$, the expected components within the first 5 Å are two peaks in the first Bi-O shell, a Bi-Ba shell, a Bi-Bi shell which should include forward scattering effects from the intervening O, and long Bi-O distances from the second O shell, which fall roughly into three distinct peaks. Figure 5 shows that additional, well-defined peaks exist at least up to 7 Å in this data. For $BaBiO_3$ we have good k-space data up to 18 $Å^{-1}$ and show the r-space data for a long Fourier transform range from 3.6 to 17.5 $Å^{-1}$ in Fig. 6.

We have fit this data over the range 1.5–5.0 Å to the above-mentioned shells but have not included multiscattering effects for the Bi-O-Bi shell. Because of the distortion of the O environment, the O is not exactly colinear with the Bi atoms and the effects of forward scattering are therefore significantly reduced. In such cases one expects a reasonable fit using a single peak for this component but the position and the amplitude will not be quite right. The extent to which they differ from the results of diffraction is a measure of the importance of this neglected contribution.

The standards we use for each of the shells are obtained by using curved-wave theory to modify the Pb-edge standards discussed in Sec. III. These standards are very similar to those used in our earlier work but more care has been taken in removing other background peaks in the standard compound data to obtain isolated single-pair standards. The fit to $BaBiO_3$ is shown as the dotted curve in Fig. 6, and the parameters are listed in Table I. In this fit, the long Bi-O peak parameters were first fixed at the values expected from the diffraction results and the short Bi-O, Bi-Ba, and Bi-Bi parameters determined. Then the constraints on the long Bi-O distances were removed; these parameters changed very little. Although the long Bi-O peaks are a relatively small correction, they are needed to obtain reasonable Bi-Ba nd Bi-Bi amplitudes.

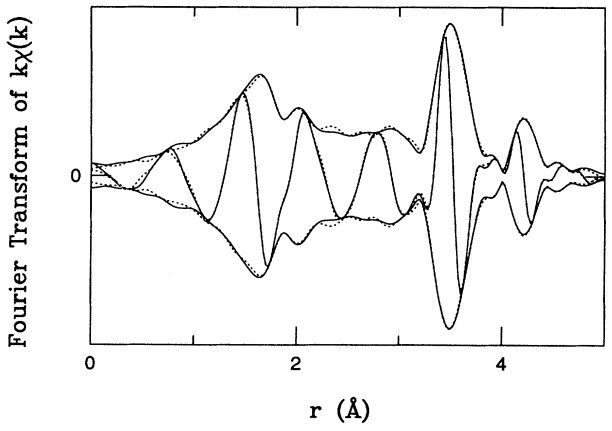

FIG. 6. XAFS in r space on the Bi L_{III} edge for $BaBiO_3$. Both the real part and the magnitude (envelope curve) of the transform are shown. A long transform range was applied: 3.6–17.5 $Å^{-1}$, Gaussian broadened by 0.3 $Å^{-1}$. The fit in the range 1.3–5.0 Å, discussed in the text with the results given in Table I, is shown as a dotted curve.

Note that the first peak in Fig. 6 shows structure consistent with two Bi-O components in the first shell. The shape and size of this peak is strongly dependent on the spacing between these peaks as shown in Fig. 7, where we have simulated the nearest-neighbor Bi-O peak for various possibilities using the Bi-O standard file. Here we use the shorter k range of 3.6–13 $Å^{-1}$, which is used for the Pb-substituted samples. The top trace is a single unbroadened standard file of amplitude 1.0. The next two traces are a sum of two unbroadened standards, each of amplitude 0.5, for two different splittings of the peaks, $\Delta r = 0.1$ and 0.18 Å. The latter corresponds to the situation in $BaBiO_3$ and shows the decreased overall amplitude (a result of interference between the two components) that is observed, as well as a change in the shape of the peak. Clearly, as the separation between the peaks decreases, we expect the amplitude to increase and the shape to change.

A review of the first peak of the data in Fig. 5 for each of the alloys shows an increase in amplitude as the Pb concentration increases and a change in shape, both of which are consistent with a decreasing Bi-O splitting. However, the amplitude is not as high as one would expect for a single, unbroadened peak, in any of the traces. We fit the data in Fig. 5 over the range 1.3–2.2 Å to both a single-peak and a double-peak structure. The pure material and the two alloys, 75% Bi and 50% Bi, show very well-separated peaks with the splitting between them decreasing slightly as the Bi concentration decreases. The improvement in the quality-of-fit parameter (R value) between the one- and two-Gaussian fits is large, a factor of 10 for $BaBiO_3$ and >5 for the 50% alloy. We obtain essentially the same results for a variety of starting parameters and also for different choices of the fit range in r. The dotted lines in Fig. 5 for the alloys are the two Gaussian fits, and the resulting structural parameters are given in Table II. Clearly, in the semiconducting samples, the tendency to have two different Bi-O bonds is

TABLE I. The distances to and average number of neighbors around the Bi atoms in $BaBiO_3$. The XAFS data, taken at 80 K, and the fit are shown in Fig. 6. Only part of the long Bi-O peak near 5.28 Å was included in the fit, accounting for the large discrepancy. Diffraction results are from Ref. 3. The uncertainties in the XAFS distances and number of neighbors are about ±1% and ±15%, respectively.

	XAFS		Diffraction	
Pairs	r (Å)	No. of neighbors	r (Å)	No. of neighbors
Bi(1)-O	2.29	6.1	2.27	6
Bi(2)-O	2.11	6.1	2.13	6
Bi-Ba	3.74	8.8	3.75–3.79	8
Bi-Bi	4.33	7.0	4.33–4.36	6
Bi-O	4.60	7.3	4.56–4.63	8
Bi-O	4.93	7.3	4.89–4.91	8
Bi-O	(5.28)	(7.3)	5.12–5.15	8

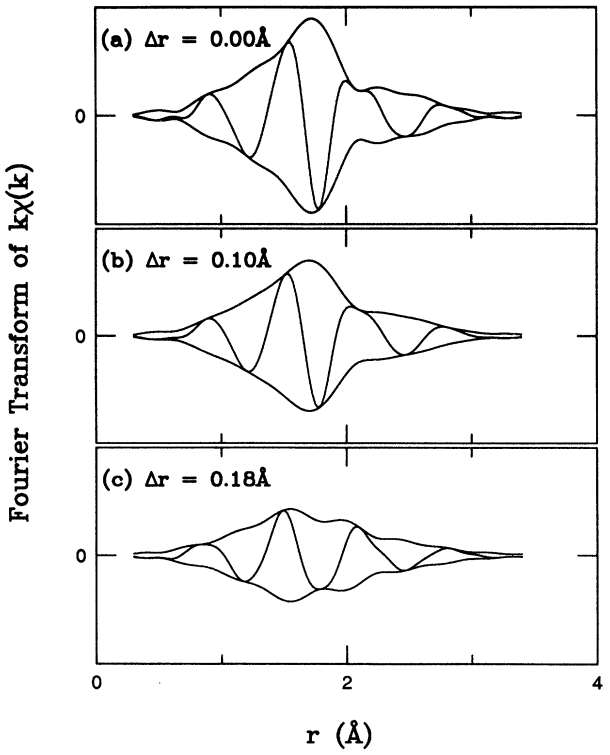

FIG. 7. The modeled XAFS in r space on the Bi L_{III} edge for six O near neighbors split into two peaks of three O neighbors each with separations of (a) $\Delta r=0$, (b) $\Delta r=0.1$ Å, and (c) $\Delta r=0.18$ Å.

strong, and the decrease in the splitting between the peaks is not large (see Table II).

For the superconducting sample, we are limited to values of r below 2.2 Å because of the increased background contribution at larger r, and the quality-of-fit parameter for the two-peak fit is about a factor of 2 lower than that for the one-Gaussian fit. For various fit ranges and starting parameters, the obtained separation of the two peaks is about 0.09–0.12 Å. A simulation of the situation using one and two Bi-O standards indicates that, for the k-space range available ($k_{max}=13$ Å^{-1}), a broadened peak and a two-peak structure are visually quite similar. The significant improvement in the R value for the two-peak fit clearly supports a two-peak structure. Because of the alloying, we might expect some disorder as a result of the variation in the local environment on the Bi sites. Usually for a homogeneous alloy this would result in slightly different values for the Pb-O and Bi-O distances. The split two-peak fit or broadened single-peak fit required to reproduce the data clearly indicate that the O neighbors do not have a single well-defined distance and indicate that the tendency for a distortion of the O about the Bi remains. We suggest that this tendency results in partially localized electrons on some of the Bi-O bonds.

VI. DISCUSSION

From the XAFS, two separate Bi-O distances have been determined in $BaBiO_3$. The values agree reasonably well with those from neutron diffraction: 2.29 and 2.11 Å compared with 2.29 and 2.12 Å reported by Cox and Sleight[1] for samples prepared in a similar way to those here; 2.26 and 2.14 Å by Thornton and Jacobson;[2] 2.26 and 2.14 Å by Chaillout *et al.*[3] Samples quenched from above 800 °C, on the other hand, gave essentially a single Bi-O distance[40] of 2.20 Å. Our results also agree well with other XAFS studies: Heald *et al.*[11] obtained 2.28 and 2.12 Å; Durmeyer *et al.*[21] 2.29 and 2.11 Å; and Salem-Sugui *et al.*,[22] 2.29 and 2.11 Å.

Upon alloying $BaBiO_3$ with Pb, the XAFS contribution from the PB edge complicates the extraction of Bi local structural parameters. However, a subtraction procedure was developed, and good fits to a two-distance Bi-O distribution (or a broad continuous distribution of distances that may be approximated by a broadened two-distance distribution) were obtained after correcting for the Pb contribution.

The general trends in these results are tabulated in Table II and shown in Fig. 8. Our data indicate that Bi tends to keep the same O environment in the alloys (including the variation in the Bi-O bond lengths) that it has

TABLE II. First-neighbor distances and average number of neighbors around the Bi and Pb atoms in Ba(Bi,Pb)O_3. The data, taken at 80 K, and these fit results are both displayed in Fig. 5 for the Bi-edge data. ⟨Bi-O⟩ is the mean Bi-O spacing and $V^{1/3}/2$ is the average near-neighbor spacing for a pseudocubic unit cell from the diffraction results of Ref. 3. The uncertainties in the XAFS Bi-O distances and number of neighbors are about ±0.02 Å and ±15%. The uncertainties in the Pb-O structure are larger due to the limited k range of the data.

	$BaBiO_3$		$BaBi_{0.75}Pb_{0.25}O_3$		$BaBi_{0.5}Pb_{0.5}O_3$		$BaBi_{0.25}Pb_{0.75}O_3$	
Pairs	r (Å)	No. of neighbors	r (Å)	No. of neighbors	r (Å)	No. of neighbors	r (Å)	No. of neighbors
Bi(1)-O	2.29	6.1	2.27	5.8	2.26	5.7	2.18	5.6
Bi(2)-O	2.11	6.1	2.11	5.8	2.12	5.7	2.09	5.6
Δr(1-2)	0.18		0.16		0.14		0.09	
⟨Bi-O⟩	2.20		2.19		2.19		2.14	
$V^{1/3}/2$	2.18	6	2.17	6	2.16	6	2.15	6
Pb-O			2.19	7.4	2.18	7.1	2.17	6.9

in the end-point compound $BaBiO_3$.[41] Neutron diffraction, however, was not able to separate two Bi-O distances in the metallic alloy.[42] The average Bi-O and Pb-O distances for a given composition are about the same or somewhat larger than the average value from the cube root of the unit-cell volume. Reports by Sleight *et al.*,[13] Kahn *et al.*,[43] and Oda *et al.*[44] give essentially the same results for the separations. An elongation of some Bi-O bonds is expected as the perovskite lattice is distorted. The Bi(Pb)-O octahedra are tipped relative to the cubic unit cell, which means that some Bi(Pb)-O separations are larger than would be the case if the octahedra were to fit untipped into undistorted perovskite cells. On the other hand, the Pb-O distances change very little with composition.

We can also compare our results with the closely related $(Ba,K)BiO_3$ alloy. XAFS studies[11,21,22] give two Bi-O distances for the semiconducting alloys, but only one distance for the superconducting one, as shown in Fig. 8. In the alloys, values of 2.13 and 2.23 Å for a 16% K sample[21] and 2.09 and 2.25 Å for a 20% K sample[22] were extracted. For the metallic $Ba_{0.6}K_{0.4}BiO_3$, the single Bi-O distance was about 2.14 Å in all studies.[11,21,22] It should also be remarked that, for the metallic alloy, there was a relatively large temperature-independent disorder in the

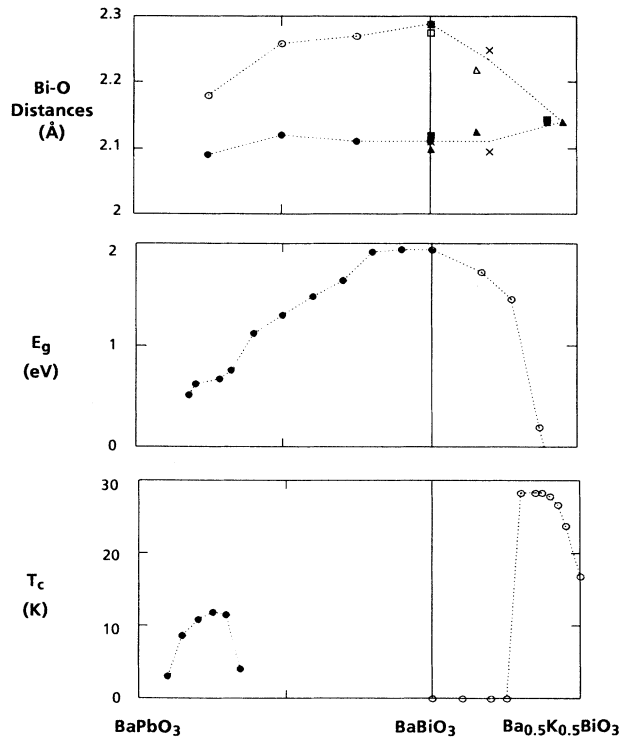

FIG. 8. The long and short Bi-O distances in $BaBi_xPb_{1-x}O_3$ and $Ba_{1-x}K_xBiO_3$ as determined by XAFS. The results on $BaBi_xPb_{1-x}O_3$ are those determined in this study, while those on $Ba_{1-x}K_xBiO_3$ are from Heald *et al.* (Ref. 11) (squares), Durmeyer *et al.* (Ref. 21) (triangles), and Salem-Sugui *et al.* (Ref. 22) (crosses). Also shown is the optical gap (Refs. 19 and 23) (middle curve) and T_c (bottom graph).

Bi-O distance. Consequently, the anharmonic behavior of the temperature dependence of the Bi-O widths might be interpreted as due to a remnant of the same type of distortions as in the undoped case.[11] We will return to other differences between the K- and Pb-doped $BaBiO_3$ that also indicate that the splitting in Bi-O distance is different for the two in the metallic state.

From our experiments, we cannot distinguish whether the Bi-O distortion is static or dynamic. The monoclinic structure of $BaBiO_3$ shows that the separation into two distances is static in that compound. One might expect the distortion to remain static within the semiconducting phase, i.e., up to 65% Pb; but in the metallic phase it is not clear if the distances fluctuate pairwise or remain permanently distorted. On the time scale of our experiment, which is of the order of 10^{-15} s, the separation into two distances (or a distribution of distances approximated by two distances) looks static.

What implications do the dual Bi-O bond lengths have? It must be connected with charge variations. In $BaBiO_3$, a Fermi-surface instability leads[9] to a monoclinic distortion with frozen breathing modes, a charge-density wave, and a semiconducting state. It has been suggested[13] that a charge disproportionation into Bi^{3+} and Bi^{5+} occurs for the two different Bi(I) and Bi(II) sites, but calculations[9] and experiments[5-8] refute this idea. It is tempting to assume that the charge variation occurs instead on the O lattice, as advocated for cuprous oxides, and arguments have been given to support this view.[11] However, it should be pointed out that the Bi-O bond has not only ionic but also covalent character.[8] Hence, the varying charge does not reside on a specific atom. We cannot determine if the charge variation occurs on the O sites or in the intermediate bond.

A semiconducting energy gap has been determined by optical measurements, as shown in Fig. 8.[18,23] It decreases with the addition of Pb but an optical pseudogap persists even in the metallic state. In the K-doped alloys, on the other hand, there is no pseudogap in the metallic state[23] (see Fig. 8). The peak in the optical conductivity (as a function of frequency) disappears in the superconducting state at 30% potassium. This would support our picture of two different Bi-O distances and local charge-density fluctuations in space (and possibly in time) in the metallic state for Pb-doped, but not K-doped alloys.

From the appearance of a new ir-active mode, the University of Tokyo group[45] proposed the formation of macroscopic clusters of ordered Bi(I) and Bi(II) configurations in the semiconducting phase, giving rise to an energy gap. Arguing from the size of the gap, one does not expect[19] the CDW coherence length to be much longer than about 10 Å. The clustering would be in accord with the theory of Rice and Sneddon,[15] who propose a condensation of real-space paired electrons. The authors speculated that, in the metallic state, the frozen breathing modes become active (i.e., have a nonzero frequency) or remain frozen over a short range below a percolation limit.

Inelastic-neutron-scattering results by Reichardt and Weber[46] indicate that there are local phonon modes associated with some lattice defect of high density. The de-

fect was proposed to be a static breathing-type distortion of the O octahedra around Bi atoms. Weber[29] has suggested that a combination of incommensurate breathing mode charge-density waves and "chemical ordering waves" on the (Bi,Pb) sublattice causes the semiconducting state for $0.35 < x < 1$. An incommensurate structure modulation in the semiconducting $(Ba,K)BiO_3$ has been seen by electron diffraction,[47] but it may be due to heating by the electron beam.[48]

Theoretical work by Sofo *et al.*,[49] who considered two interpenetrating lattices of disproportionated Bi, could model a semiconducting state with a CDW gap and a metallic state for the Pb-doped alloy where the disproportionation was not inhibited but gives rise to a pseudogap. Inada and Ishii[50] also took into account dynamic breathing modes and obtained similar results. They found that the breathing mode was not completely frozen out in the metallic state. A charge-ordered, insulating state appeared above a critical concentration of $x = 0.37$ when the Pb bands no longer overlap the split Bi bands. In this picture, one expects a pseudogap to remain if the Pb-band density of state is considerably smaller than the Bi-band density of states.

A much higher Pb than K concentration is needed to transform the semiconducting $BaBiO_3$ into a metallic state. This is not surprising since Pb has the same formal valence (4+) as that of the Bi in $BaBiO_3$ while K has a different valence from Ba (1+ versus 2+). The effective charge carrier concentration in the metallic K-doped compound will consequently change more rapidly with substitution than that of the Pb-substituted alloy. The conduction is along Bi-O orbitals; hence, the Pb dopants will go into the conducting paths and the (Bi,Pb) disorder will add to the localization tendency of electrons. This is not the case for K (or Rb) doping. Sugai and coworkers[51] conclude from Raman-scattering experiments that the extend of the itinerant electron wave function is much larger in the K-doped than the Pb-doped oxide. This helps to achieve a high electron concentration and a higher T_c before developing a CDW semiconducting state. The K- and Pb-doped bismuth oxides thus have important differences.

For the superconducting alloys, Batlogg *et al.*,[24] argue that the electron-phonon mechanism is not sufficient to cause superconductivity in the doped barium-bismuth oxides. From critical field measurements, they extract an electron-phonon coupling parameter λ of 0.6–0.8. This is considerably lower than the value of λ of about 1.5 to 2 that one would obtain applying the McMillan equations[52] and a Debye temperature of 150 to 200 K. On the other hand, an isotope effect close to the BCS value and phonon-induced structure in tunneling curves point to the importance of the electron-phonon coupling.[53,54]

Theoretical estimates[25–27] of the superconducting transition temperature, T_c, using band-structure calculation and the McMillan approximation or the full Eliashberg theory, have shown that it is possible to explain the superconductivity of $(Ba,K)(Bi,Pb)O_3$ within the electron-phonon coupling mechanism. Two of the studies require a large λ, one a small value. Papaconstantopoulos *et al.*[26] find that an average phonon frequency corresponding to 200–400 K and a strong coupling λ of 2.4 could result in a T_c of 26 K. Hamada *et al.*,[25] used a fairly large λ of about 3 to obtain 30 K. The coupling contribution from Bi phonon modes was much smaller than from O ones, whereas it was negligible from Ba modes.

Shirai *et al.*,[27] found that the longitudinal optical oxygen stretching (or breathing) mode vibration was strongly renormalized and broadened. That may explain why an optical phonon band was not detected at about 40 meV by inelastic neutron scattering.[46] For relatively high-frequency phonons, they[27] obtained a T_c of 30 K for $(Ba,K)BiO_3$ with a λ of 0.7–1 (λ becomes small when high-frequency phonons are dominant). Furthermore, they got a gap to transition temperature ratio $2\Delta/k_B T_c$ of about 3.6, i.e., a weak-coupling value. Thus, their theoretical results compare well with experiment for $(Ba,K)BiO_3$.

From the temperature dependence of the XAFS, we have previously[10] extracted Einstein temperature of about 500 K for the Bi(Pb)-O local vibrational modes. 500 K corresponds to about 43 meV, which is in good agreement with the results above and with neutron scattering[46,55] and Raman results[56] (assuming that the 320-cm^{-1} peak is the breathing mode). Heald *et al.*[11] were able to separate the temperature dependence of the two Bi-O distances and found characteristic temperatures of about 490 and 340 K for the short (stiff) and long (soft) bonds, respectively, in $BaBiO_3$. Also in the metallic K-doped compound the dominating longitudinal stretching mode had a characteristic temperature of about 500 K.

For $(Ba,K)BiO_3$, the electron-phonon mechanism seems to describe superconductivity well, but for $Ba(Bi,Pb)O_3$, Shirai *et al.*[27] got too low a T_c, of the order of a few K instead of 13 K. The discrepancy might be remove by taking into account a random distribution of Bi for Pb (which was not done in the calculations). However, one may also speculate on other causes of the difference between the K- and Pb-doped alloys as well as on mechanisms that enhance the electron-phonon coupling in these alloys. Several mechanisms have been proposed to explain the superconductivity of doped $BaBiO_3$, including excitons, biexcitons, plasmons, bipolarons, charge-density fluctuations, and real-space pairing.

Generally, one would expect a CDW to be detrimental to superconductivity. It would localize charge and prevent the formation of Cooper pairs in k space.[15] However, a strong electron-phonon coupling strength would promote both superconductivity and the formation of charge-density fluctuations. Ting *et al.*[33] proposed an enhancement of superconductivity due to the softening of the oxygen breathing modes around Bi atoms at compositions near a CDW instability. Ichimura *et al.*[34] argued that an imperfect nesting of a CDW would lead to a large density of states with an enhanced T_c and a pseudogap in the superconducting state. A density-of-states enhancement mechanism was also proposed by Machida.[57] Yu *et al.*,[58] however, argue against an enhancement of the density of states in a doped compound where the CDW

amplitude would diminish with doping. Our results suggests that a local, rather than a long-range, CDW exists in the superconducting state.

In our case, charge-density fluctuations and varying Bi-O lengths are connected. The electrons are directed along the Bi-O bonds; they are partly localized, partly itinerant. An extra conduction electron will modify the charge distribution and the bond length, giving rise to relatively high-frequency phonons. Hence, the electron-phonon mediated interaction between electron pairs may be modified by coupling to localized distorted regions (polaron type[59]). This may promote superconductivity.

It is natural to ask if near-neighbor variations from site to site also exist in the high-T_c cuprate oxides. Experimentally, the situation is complicated by the fact that the Cu-O bonds have different lengths in different directions in a pyramidal configuration. One possibility may be to study the T phase, where copper atoms sit in equivalent square oxygen environments. A charge-density variation would be of considerable interest if found, as the coupling mechanism in copper oxides is proposed by many authors to be connected with a spin-density fluctuation rather than a charge-density fluctuation.

VII. CONCLUSION

The extraction of information from the XAFS of the Bi edge in Pb-rich $Ba(Bi,Pb)O_3$ is complicated by the proximity of the Pb absorption edge. The XAFS from the Pb edge is strong and interferes with the Bi XAFS. We have used a procedure for extending the XAFS on the Pb edge to energies in the region above the Bi edge. This procedure allows us to subtract the contribution of the Pb-edge XAFS for the Bi-edge data, allowing quantitative analysis of the Bi-edge XAFS.

Two Bi-O distances, 0.18 Å apart, could be extracted from the XAFS data for $BaBiO_3$. The separation remains when Pb is substituted for Bi in the semiconducting phase. For the superconducting alloy, two Bi-O peaks with a separation of about 0.12 Å are found. The Bi-O distances in the alloys are different from the Pb-O separation, indicating that the Bi and Pb atoms prefer the local environments of the end constituents. The observation of two Bi-O distances is consistent with the pseudogap in the 25% Bi alloy and supports the picture of a local CDW in the metallic and superconducting phase.

ACKNOWLEDGMENTS

The experiments were performed at the Stanford Synchrotron Radiation Laboratory, which is supported by the U.S. Department of Energy, Office of Basic Sciences, and the National Institutes of Health, Biotechnology Division. Support was obtained from the Swedish Natural Science Research Council and the U.S. Air Force Office of Scientific Research. The work of F.G.B. and G.G.L. is supported by NSF Grant No. DMR-90-04325.

[1]D. E. Cox and A. W. Sleight, Acta. Crystallogr. B **35**, 1 (1979).
[2]G. Thornton and A. J. Jacobson, Acta Crystallogr. B **34**, 351 (1978).
[3]C. Chaillout, A. Santoro, J. P. Remeika, A. S. Cooper, G. P. Espinosa, and N. Marezio, Solid State Commun. **65**, 1363 (1988).
[4]Shiyou Pei, N. J. Zaluzec, J. D. Jorgensen, B. Dabrowski, D. G. Hinks, A. W. Mitchell, and D. R. Richards, Phys. Rev. B **39**, 811 (1989).
[5]G. K. Wertheim, J. P. Remeika, and D. N. E. Buchanan, Phys. Rev. B **26**, 2120 (1982).
[6]M. S. Hegde, P. Barboux, C. C. Chang, J. M. Tarascon, T. Venkatesan, X. D. Wu, and A. Inam, Phys. Rev. B **39**, 4752 (1989).
[7]Y. Jeon, G. Liang, J. Chen, M. Croft, M. W. Rucknan, D. Di Marzio, and M. S. Hegde, Phys. Rev. B **41**, 4066 (1990).
[8]Z.-X. Shen, P. A. P. Lindberg, B. O. Wells, D. S. Dessau, A. Borg, I. Lindau, W. E. Spicer, W. P. Ellis, G. H. Kwei, K. C. Ott, J.-S. Kang, and J. W. Allen, Phys. Rev. B **40**, 6912 (1989).
[9]L. F. Mattheiss and D. R. Hamann, Phys. Rev. B **28**, 4227 (1983).
[10]J. B. Boyce, F. G. Bridges, T. Claeson, T. H. Geballe, and J. M. Remeika, Phys. Rev. B **41**, 6306 (1990).
[11]S. M. Heald, D. DiMarzio, M. Croft, M. S. Hegde, S. Li, and M. Greenblatt, Phys. Rev. B **40**, 8828 (1989).
[12]G. U. Kulkarni, V. Vijayakrishnan, G. Ranga Rao, Ram Seshadri, and C. N. R. Rao, Appl. Phys. Lett. **57**, 1823 (1990).
[13]A. W. Sleight, J. L. Gillson, and P. E. Bierstedt, Solid State Commun. **17**, 27 (1975).
[14]For a review of superconductivity and metal-semiconductor transition, see S. Uchida, K. Kitazasa, and S. Tanaka, Phase Trans. **8**, 95 (1987).
[15]T. M. Rice and L. Sneddon, Phys. Rev. Lett. **47**, 689 (1981).
[16]D. Yoshioka and H. Fukuyama, J. Phys. Soc. Jpn. **54**, 2996 (1985).
[17]E. Jurczek and T. M. Rice, Europhys. Lett. **1**, 225 (1986).
[18]S. Tajima, S. Ushida, A. Masaki, H. Takagi, K. Kitazawa, S. Tanaka, and A. Katsui, Phys. Rev. B **32**, 6302 (1985); S. Tajima, S. Uchida, A. Masaki, H. Takagi, K. Kitazawa, S. Tanaka, and S. Sugai, *ibid.* **35**, 696 (1987).
[19]T. Claeson, J. B. Boyce, F. G. Bridges, T. H. Geballe, J. M. Remeika, and A. W. Sleight, Physica C **162-164**, 544 (1989).
[20]R. J. Cava, B. Batlogg, J. J. Kajewski, R. Farrow, L. W. Rupp, Jr., A. E. White, K. Short, W. F. Peck, and T. Kometani, Nature **332**, 814 (1988); L. F. Mattheiss, E. M. Gyorgy, and D. W. Johnson, Jr., Phys. Rev. B **37**, 3745 (1988).
[21]O. Durmeyer, E. Beaurepaire, J. P. Kappler, C. Hornick, and M. Drillon, J. Less Common Met. **164&165**, 934 (1990).
[22]S. Salem-Sugui, Jr., E. E. Alp, S. M. Mini, M. Ramanathan, J. C. Campuzano, G. Jennings, M. Faiz, S. Pei, B. Dabrowski, Y. Zheng, D. R. Richards, and D. G. Hinks, Phys. Rev. B **43**, 5511 (1991).
[23]H. Sato, S. Tajima, H. Takagi, and S. Uchida, Nature **338**, 241 (1989); Physica C **162-164**, 1121 (1989).
[24]B. Batlogg, R. J. Cava, L. W. Rupp, Jr., A. M. Mujsce, J. J.

Krajewski, J. P. Remeika, W. F. Peck, Jr., A. S. Cooper, and G. P. Espinosa, Phys. Rev. Lett. **61**, 1670 (1988).
[25]N. Hamada, S. Massidda, A. J. Freeman, and J. Redinger, Phys. Rev. B **40**, 4442 (1989).
[26]D. A. Papaconstantopoulos, A. Pasturel, J. P. Julien, and F. Cyrot-Lackmann, Phys. Rev. B **40**, 8844 (1989).
[27]M. Shirai, N. Suzuki, and K. Motizuki, J. Phys.: Condens. Matter **2**, 3553 (1990).
[28]A. Aleksandrov and J. Ranninger, Phys. Rev. B **23**, 1796 (1981).
[29]W. Weber, Jpn. J. Appl. Phys. **26**, Suppl. 26-3, 981 (1987).
[30]C. M. Varma, S. Schmitt-Rink, and E. Abrahams, Solid State Commun. **62**, 681 (1987).
[31]C. M. Varma, Phys. Rev. Lett. **61**, 2713 (1988).
[32]M. D. Nunez Regueiro and A. A. Aligia, Phys. Rev. Lett. **61**, 1889 (1988).
[33]C. S. Ting, X. Y. Chen, and Z. Y. Weng, Mod. Phys. Lett. B **3**, 1267 (1989).
[34]M. Ichimura, M. Fujita, and K. Nakao, Phys. Rev. B **43**, 175 (1991).
[35]T. M. Hayes and J. B. Boyce, in *Solid State Physics,* edited by H. Ehrenreich, F. Seitz, and D. Turnbull (Academic, New York, 1982), Vol. 37, p. 137.
[36]R. W. G. Wyckoff, *Crystal Structures* (Interscience, New York, 1963).
[37]J. B. Boyce, J. C. Mikkelsen, Jr., F. Bridges, and T. Egami, Phys. Rev. B **33**, 7314 (1986).
[38]J. Mustre, Y. Yacoby, E. A. Stern, and J. J. Rehr, Phys. Rev. **42**, 10 843 (1990); A. G. McKale, B. W. Veal, A. P. Paulikas, S.-K. Chan, and G. S. Knapp, J. Am. Chem. Soc. **110**, 3763 (1988).
[39]J. B. Boyce, F. Bridges, T. Claeson, and M. Nygren, Phys. Rev. B **39**, 6555 (1989).
[40]C. Chaillout, J. P. Remeika, A. Santoro, and M. Marezio, Solid State Commum. **56**, 829 (1985).
[41]J. B. Boyce and J. C. Mikkelsen, in *Ternary and Multinary Compounds,* edited by S. K. Deb and A. Zunder (Materials Research Society, Pittsburgh, 1987), p. 359.
[42]D. E. Cox and A. W. Sleight, in *Proceedings of the Conference on Neutron Scattering* (U.S. Dept. of Commerce, Gatlinburg, TN, 1976), p. 45.
[43]Y. Khan, K. Nahm, M. Rosenberg, and H. Willner, Phys. Status Solidi A **39**, 79 (1977).
[44]M. Oda, Y. Hidaka, A. Katsui, and T. Murakami, Solid State Commun. **55**, 423 (1985); **60**, 897 (1986).
[45]S. Uchida, S. Tajima, A. Masaki, S. Sugai, K. Kitazawa, and S. Tanaka, J. Phys. Soc. Jpn. **54**, 4395 (1985).
[46]W. Reichardt and W. Weber, Jpn. J. Appl. Phys. **26**, Suppl. 26-3, 1121 (1987).
[47]See Ref. 4.
[48]E. A. Hewat, C. Chaillout, M. Godinho, M. F. Gorius, and M. Marezio, Physica C **157**, 228 (1989).
[49]O. Sofo, A. A. Aligia, and M. D. Nunez Reguerio, Phys. Rev. B **40**, 6955 (1989).
[50]Y. Inada and C. Ishii, J. Phys. Soc. Jpn. **59**, 2124 (1990).
[51]S. Sugai, Y. Enomoto, and T. Murakami, Solid State Commun. **72**, 1193 (1989).
[52]W. L. McMillan, Phys. Rev. **167**, 331 (1968).
[53]D. G. Hinks, B. Dabrowski, D. R. Richards, J. D. Jorgensen, S. Pei, and J. F. Zasadzinski, Physica C **162-164**, 1405 (1989).
[54]B. Batlogg, Physica B **126**, 275 (1984).
[55]C.-K. Loong, P. Vashishta, R. K. Kalia, M. H. Degani, D. L. Price, J. D. Jorgensen, D. G. Hinks, B. Dabrowski, A. W. Mitchell, D. R. Richards, and Y. Zheng, Phys. Rev. Lett. **62**, 2628 (1989).
[56]S. Sugai, Jpn. J. Appl. Phys. **26**, Suppl. **26-3**, 1123 (1987).
[57]K. Machida, Physica C **156**, 276 (1988).
[58]J. Yu, X. Y. Chen, and W. P. Su, Phys. Rev. B **41**, 344 (1990).
[59]S. Sugai, Solid State Commun. **72**, 1187 (1989).